e-Polymers **2007**, no. 139

http://www.e-polymers.org

ISSN 1618-7229

Structure and Mechanical Behavior of Isotactic Polypropylene Composites Filled with Silver Nanoparticles

Sie Chin Tjong,[1]* *Suping Bao*[2]

[1*]Department of Physics and Materials Science, City University of Hong Kong, Tat Chee Avenue, Kowloon, Hong Kong; Fax: (852) 2788 7830; e-mail: aptjong@cityu.edu.hk

[2]Department of Physics and Materials Science, City University of Hong Kong,Tat Chee Avenue, Kowloon, Hong Kong

(Received: 13 February, 2007; published: 26 November, 2007)

Abstract: Isotactic polypropylene (PP) nanocomposites containing 0.1, 0.3, 0.5 and 1.0 wt % silver (Ag) nanoparticles were prepared via melt compounding in a twin-screw extruder followed by injection molding The effects of the Ag nanoparticle additions on the structure and mechanical behavior of PP were studied using DSC, WXRD, optical microscopy, tensile and Izod impact techniques. DSC and WXRD measurements showed that the addition of only 0.1 wt% Ag nanoparticles promote the formation of β-form PP. Further increasing Ag content would not lead to additional increase of the β-PP phase content. The induced β-form PP phase is beneficial to enhance the impact strength and tensile ductility of the PP/Ag nanocomposites.

Introduction

Isotactic polypropylene (PP) is used extensively in various application fields such as food packaging, medical care, automobile and other industrial sectors. The mechanical performances of PP can be further enhanced by adding inorganic fillers. The most commonly used low-cost fillers for PP include talc, calcium carbonate, short glass fiber and mica [1-6]. However, a large volume fraction of fillers, ca 25-30 % is needed to achieve desired mechanical properties. Such large volume content of fillers with micrometric sizes can lead to poor processability and severe wear of processing facilities. Moreover, the incorporation of micrometer fillers to PP generally leads to a large reduction in their tensile ductility and impact toughness. In recent years, various inorganic and ceramic nanofillers of lower volume contents (~ 2- 10%) are introduced into PP to meet increasing demands for special applications. Considerable improvements in tensile strength and ductility can be achieved in PP using nanofiller reinforcements [7-10].

The mechanical performance of crystalline thermoplastics depends greatly on the microstructure which in turn relates to their crystallization behavior including crystallite morphology and degree of crystallinity. PP, the typical crystalline polymer, is known to exhibit three crystallographic forms, namely monoclinic α-form, trigonal β-form and triclinic γ-form [11]. The formation of those crystalline forms is critically dependent upon the crystallization condition, molecular weight and tacticity of PP.

The α-form PP is the most stable and also the most prevalent one. The β-form PP is observed occasionally and appears as a minor constituent of PP. It is well known that the β-form PP is beneficial to enhance the impact toughness of PP at the expense of yield strength. High contents of β-form PP can be produced during directional crystallization in a high temperature gradient field [12], shear-induced crystallization [13] or the addition of specific nucleating agents such as quinacridone dye, triphenodithiazine, pimelic acid or calcium carbonate [14, 15].

The incorporation of nanoparticles to enhance polymer performance has generated considerable research interest in the past decade. Silver, a non-toxic natural inorganic metal, can eliminate many harmful microorganisms against human body. It is a very good antibacterial agent and widely added to polymers to obtain bactericidal activity. Some studies have been conducted on the excellent antibiotic property of the polymer composites filled with Ag nanoparticles [16, 17]. However, little information is available in the literature relating the structure and mechanical property of the PP composites filled with Ag nanoparticles. In the present study, the structure of PP filled with Ag nanoparticles prepared by melt compounding and injection molding was investigated. The effect of Ag nanoparticle additions on the mechanical property of PP is also discussed.

Results and Discussion

Structure

-Dispersion of nanoparticles in PP matrix

Figure 1 shows representative TEM micrograph of the PP/1.0 wt% Ag nanocomposites. The silver nanoparticles tend to link together to form small clusters. However, few isolated nanoparticles can still be recognized from the TEM image. Both the clusters and isolated nanoparticles are well dispersed within PP matrix.

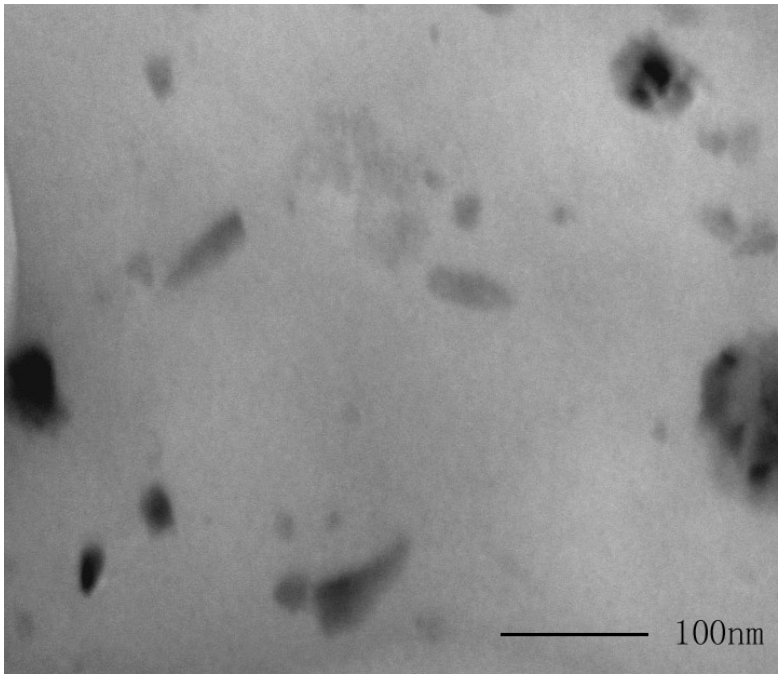

Fig. 1. TEM micrograph of PP/1.0wt% Ag nanocomposites.

Melting and crystallization behavior

Figure 2 shows the DSC melting curves of pure PP and PP nanocomposites filled with Ag nanoparticles at a heating rate of 10 °C min^{-1}. Pure PP shows a fusion peak at 162.22 °C, corresponding to the melting peak of α-phase crystals (T_m^{α}). The incorporation of Ag nanoparticles into PP leads to the presence of an extra fusion peak at ~ 148 °C. This peak can be assigned to the melting peak of β-PP crystals (T_m^{β}). This is because the β-crystalline form of PP often exhibits a lower melting point (~150 °C) compared to α-PP [18-20]. Furthermore, a shoulder peak appears between the two fusion peaks in the DSC heating scan of PP composites, possibly due to the conversion of the β-PP to the α-PP during heating [21].

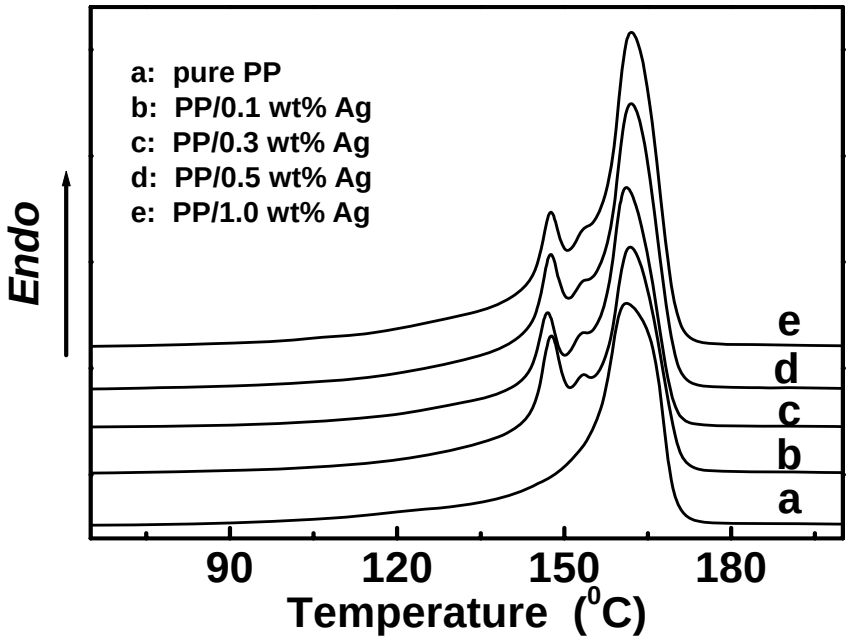

Fig. 2. Melting curves of pure PP and PP/Ag nanocomposites at a heating rate of 10 °C min^{-1}

The degree of crystallinity, ϕ_{α}, of α-PP can be calculated according to the following equation:

$$\phi_{\alpha} = \frac{\Delta H_{\alpha}}{\Delta H^{0}} \times 100\% \quad (1)$$

where ΔH_{α} is the fusion heat due to the α-PP crystals in the sample and ΔH^{0} is the standard fusion heat of 100% crystalline isotactic PP taken as 209J/g from the literature [22]. Similarly, the degree of crystallinity, ϕ_{β},of the β-PP can be determined by:

$$\phi_{\beta} = \frac{\Delta H_{\beta}}{\Delta H^{0}} \times 100\% \quad (2)$$

where ΔH_{β} is the fusion heat due to the β-PP phase crystals. The fraction percentage of β-form PP, X_{β}, can be evaluated from the following equation:

$$X_\beta = \frac{\phi_\beta}{\phi_\alpha + \phi_\beta} \times 100\% \quad (3)$$

All DSC parameters determined are summarized in Table 1. Apparently, the addition of only 0.1 wt. % Ag to PP induces the formation of β-PP phase of 27.60 %. Further increasing Ag content does not lead to additional increase of the β-PP phase content. It is noted that the melting temperatures of α- phase of the PP nanocomposites is close to that of pure PP (~161 °C).This implies that the Ag nanoparticle additions have little effect on the melting of α-PP phase crystals.

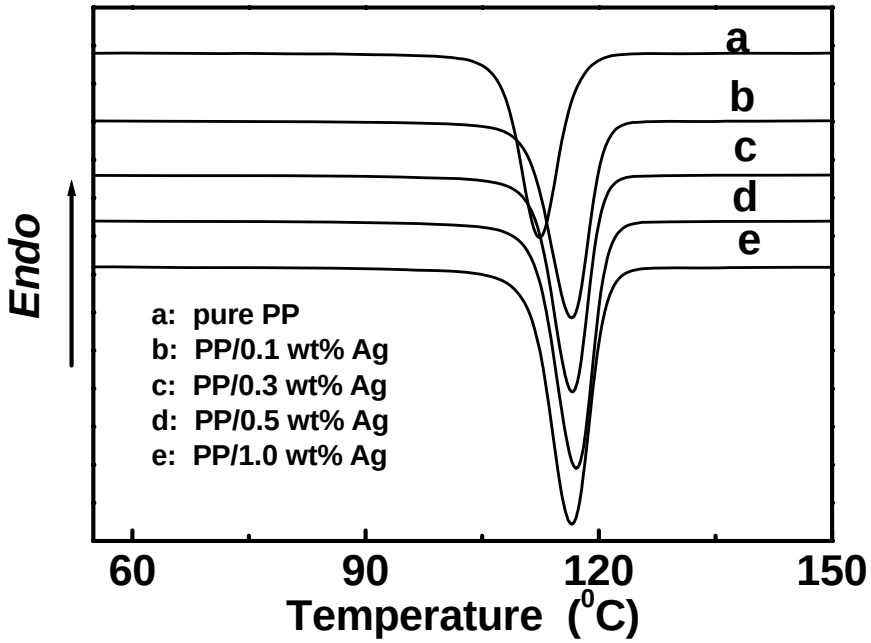

Fig. 3. DSC traces of pure PP and PP/Ag nanocomposites at a cooling rate of 10 °C min^{-1}

Tab. 1. DSC results of pure PP and PP/Ag nanocomposites.

Specimens	T_m^α (°C)	T_m^β (°C)	ϕ_α (%)	ϕ_β (%)	X_β (%)	T_c (°C)
PP	161.22	-	40.87	-	-	112.39
PP/0.1wt%Ag	161.96	147.68	34.21	13.04	27.60	116.50
PP/0.3wt%Ag	161.39	146.99	38.35	14.54	27.49	116.61
PP/0.5wt%Ag	161.97	147.56	35.59	13.54	27.56	117.01
PP/1.0wt%Ag	162.00	147.09	37.48	14.09	27.32	116.53

The crystallization curves of pure PP and PP/Ag nanocomposites at a cooling rate of 10 °C min^{-1} are shown in Figure 3. The results indicate that the crystallization peak temperature (T_c) of PP increases from ~ 112 to ~ 117 °C due to Ag additions (Table 1). Hence, the incorporation of Ag nanoparticles enhances the crystallization temperature. Therefore, the Ag nanoparticles play an important role during the crystallization process of PP. They act as effective heterogeneous nucleation agents to facilitate PP crystallization. Obviously, heterogeneous nucleating effect of Ag

nanoparticles causes an increase in the crystallization temperature of PP nanocomposites. Chae et al. [23] also reported that the inclusions of Ag nanoparticles exhibit a nucleation effect on the crystallization of PP.

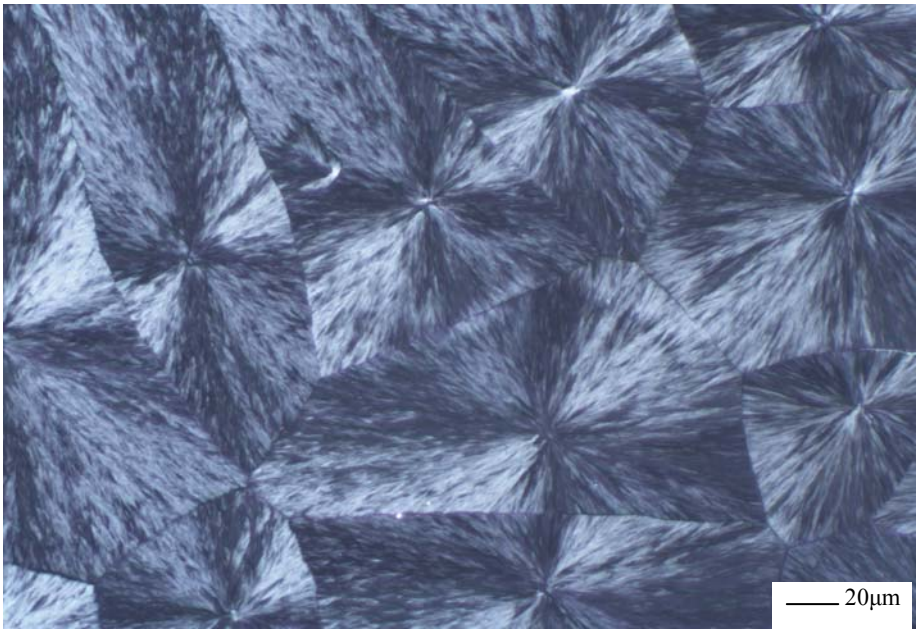

(a)

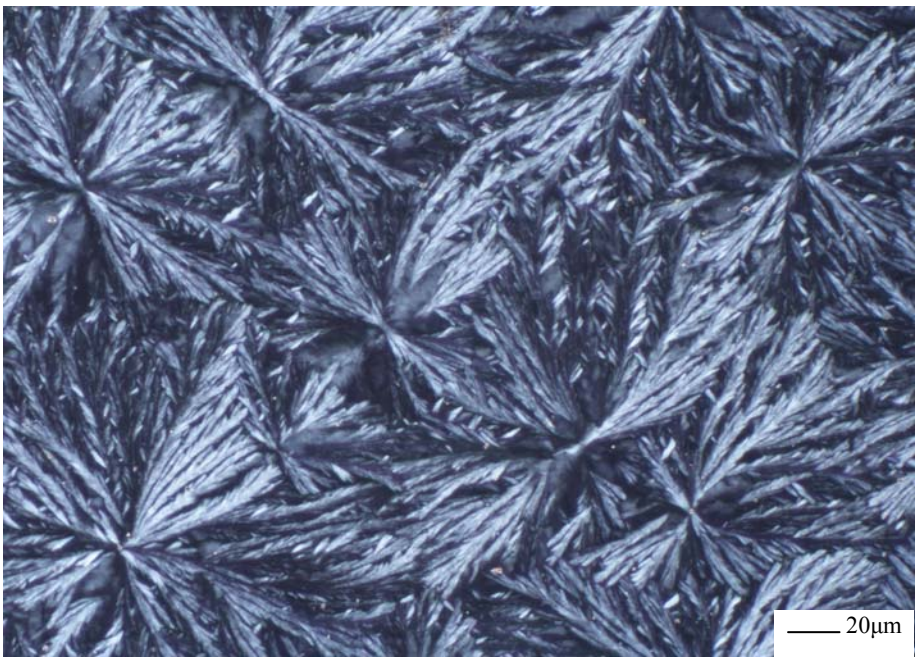

(b)

Fig. 4. Polarizing optical micrographs of (a) pure PP and (b) PP/0.3 wt% Ag nanocomposites.

Figures 4 (a)- (b) show the polarizing optical micrographs (POM) of pure PP and PP composite filled with 0.3 wt% Ag nanoparticles, respectively. It can be seen that that the nucleation of pure PP is homogenous; the growth of lamellae radiates from the center outward in all directions (Fig.4 (a)), which is the typical spherulite shape of α-

form PP. The Ag nanoparticles provide additional sites for the crystal nucleation and facilitate formation of a sheaf-like spherulitic structure (β-form) (white circles in Fig. 4 (b)). Furthermore, the growing spherulite extends across the boundary into the neighbor spherulites. This results in the formation of interconnected boundaries, which are different from distinct boundaries of the spherulites of α-form PP.

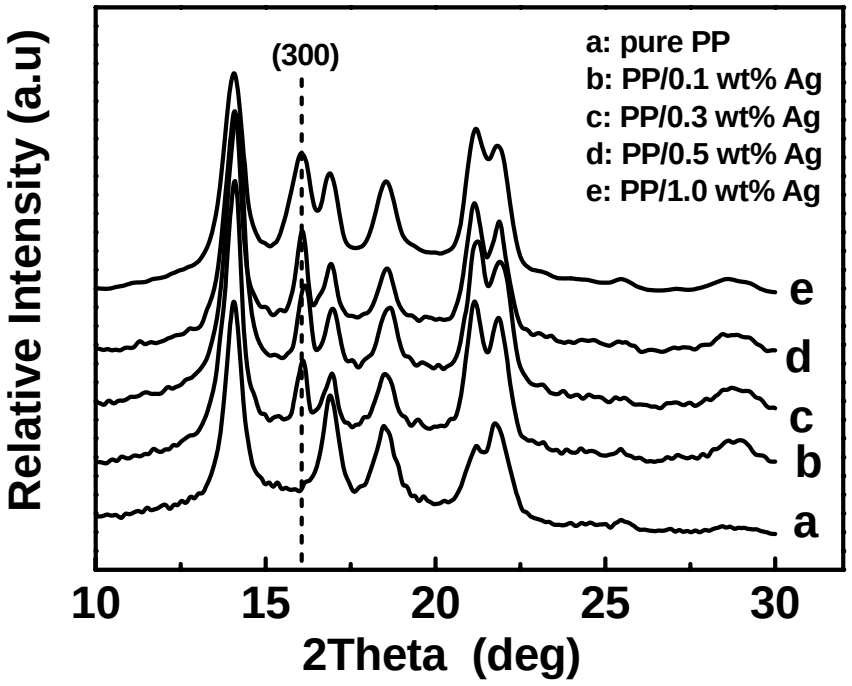

Fig. 5. WXRD patterns of extruded PP and PP/Ag nanocomposites.

Figure 5 shows the WXRD patterns of the extruded pure PP and PP/Ag composites. Pure PP presents five strong characteristic peaks of α-PP. The peaks at 2θ = 14.1˚, 16.9˚, 18.5˚, 21.2˚ and 21.8˚, corresponding to primary diffraction of the (110), (040), (130), (111) and (041) α-phase crystals respectively. All diffraction peaks of the α-phase crystals for PP/Ag composites are observed at similar Bragg angles. In addition to the diffraction peaks of the α-PP, the PP/Ag nanocomposites exhibit another distinct diffraction peak at 2θ = 16.0˚, which can be ascribed to the (300) crystal plane of β-PP. For pure PP, the intensity of diffraction peak at 21.2˚ is lower than that of peak at 21.8˚. A reverse trend in such peak intensities is found in the PP nanocomposites, i.e the diffraction peak at 21.2˚ exhibits higher intensity. This is because the (130) diffracting peak of the β-form PP located at 21.2 ˚ overlaps with the (111) peak of α-form PP.

To obtain the relative amount of the β-form PP from the WXRD patterns, an empirical parameter *k* can be used [24, 25]:

$$k = \frac{H_{300}}{H_{300} + H_{110} + H_{040} + H_{130}} \quad (4)$$

where H_{110}, H_{040} and H_{130} are the heights of the three strong diffraction peaks of α-PP, and H_{300} is that of the strongest characteristic β-PP. Taking into account the

existence of an amorphous phase, the crystalline diffraction peaks should be isolated prior to the calculation of the *k* value.

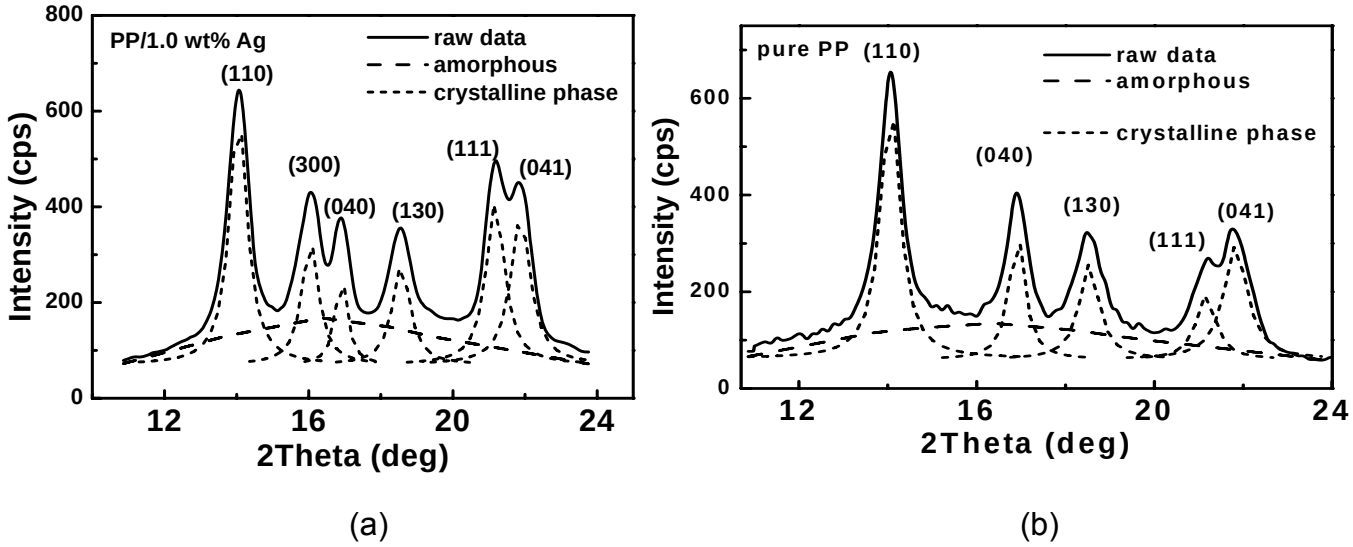

(a) (b)

Fig. 6. Representative WXRD patterns of (a) pure PP and (b) PP/1.0 wt% Ag nanocomposites. The profile fitting technique is used to deconvolute the diffracting peaks into crystalline and amorphous phases of PP.

Figs.6 (a)-(b) show typical profile fitting diffraction peaks for pure PP and PP/1.0 wt% Ag nanocomposites. The *k* values obtained are listed in Table 2. It is noted that the relative amount of β-PP calculated is lower compared to the DSC results. This is because the techniques of DSC and WXRD are based on different physical concepts. The values of *k* and X_β obtained from WXRD cannot be compared directly. Nevertheless, both methods demonstrate that higher filler content has little effect on the relative amount of the β- PP formed.

Tab. 2. Relative amount of β-form PP (*k* value) in PP/ Ag nanocomposites.

Ag content (wt%) / *k*-value	0.1	0.3	0.5	1.0
k_1	19.92 %	19.75 %	20.91 %	20.72 %
k_2	19.19 %	18.70 %	19.82 %	18.75 %
k_3	19.42 %	19.09 %	19.04 %	19.37 %

k_1: calculated *k* value for extruded samples
k_2: calculated *k* value for the skin section of injection samples
k_3: calculated *k* value for the core section of injection samples

It is generally recognized that a complex condition of stress and thermal gradients develop in polymers during injection molding. This may affect the nucleation and crystallization behavior of crystalline polymers. The WXRD patterns of PP composites filled with 0.3 wt% and 0.5 wt% Ag nanoparticles at different regions of the injection samples are depicted in Figs. 7 (a) and (b), respectively. There is little change in the diffraction angles of crystalline peaks for the specimens in different

regions of injection molded plaques. However, the intensities of the (110) and (040) α-PP peaks vary from the skin to core section. In contrast, the intensity of (300) β-PP peak shows little change. For the core section of injection molded specimens, their WXRD patterns are very similar to those of the extrusion specimens, i.e. the (110) crystalline peak is the strongest among five crystalline peaks of the α-PP phase. However, the intensity of (040) peak is much higher than that of (110) peak at the skin section of injection molded specimens.

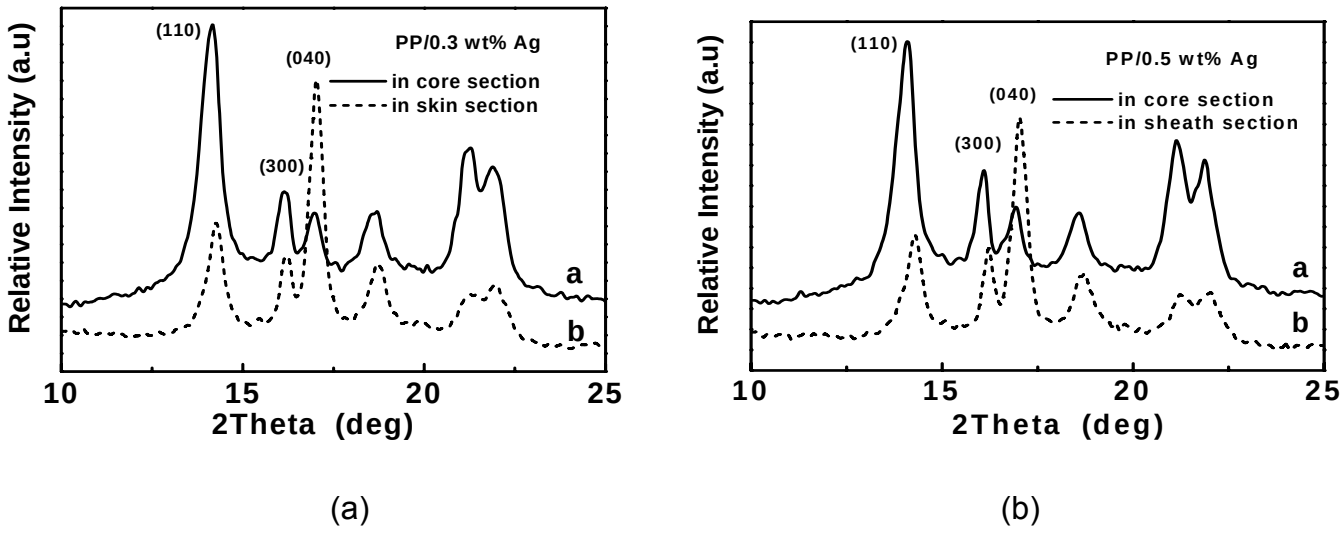

Fig. 7. WXRD patterns of (a) PP/0.3 wt% Ag and (b) PP/0.5wt% Ag nanocomposites at different sections of injection molded specimens.

The diffraction intensity is known to be dependent upon the size of crystallites lying along three crystallographic directions. For the α-PP with a monoclinic structure, the (040) crystallites are oriented in the *b*-axis direction. In general, high shear stress prevails near the mold surface during injection process. The shear stress enhances crystallization of the PP chain molecules in the *b*-axis direction at the surface of the injection sample. From Eq.4, the relative amount of β-form PP in the skin and core sections of injection molded specimens (k_1 and k_2) can be determined. The results are also listed in Table 2.

Mechanism of β-PP nucleation

The nucleation mechanisms of β-PP associated with the incorporation of β-nucleating agents have been studied by several researchers. For example, Lotz and coworkers [26-28] proposed a “dimensional lattice matching theory” on the basis of analysis of the structural relationships between nucleating agents and β-PP. A lattice matching between the c-axis periodicity of PP ($6.5\,\dot{A}$) and a corresponding distance in the substrate crystal face of nucleating agent are needed for epitaxial crystallization of β-PP. However, the “dimensional lattice matching theory” cannot be applied to all β-nucleating agents. Garbarczyk [29] reported that the shape of β-nucleating agents plays an important role on the β-PP formation. Nucleators with plat or lumpish morphology favor the growth of β-PP. In contrast, needle-like morphology is less effective for the formation of β-PP.

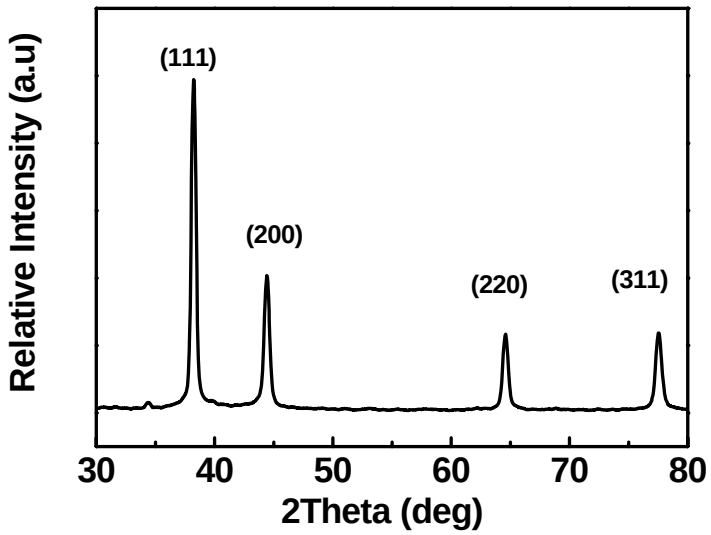

Fig. 8. X-ray diffraction pattern of silver nanoparticles.

We now consider the validity of Lotz's mechanism for the PP composites reinforced with Ag nanoparticles. Fig. 8 shows the X-ray powder diffraction diagram of silver nanoparticles. The lattice parameter of silver nanoparticles having a face-centered cubic structure ($a = b = c$) is determined to be 4.07 $\dot{A}$. It appears that this value is smaller than that required for "dimensional lattice matching theory". As mentioned above, silver fillers disperse as small clusters and independent nanoparticles (Fig. 14). The shape of silver nanoparticles may play an important role for β-PP nucleation. To get further insight into the nucleation process of β-PP, optical and scanning electron microscopic methods are used to examine the morphology of the spherulites developed in the composite during the early stage of crystallization (Figs. 9 and 10).

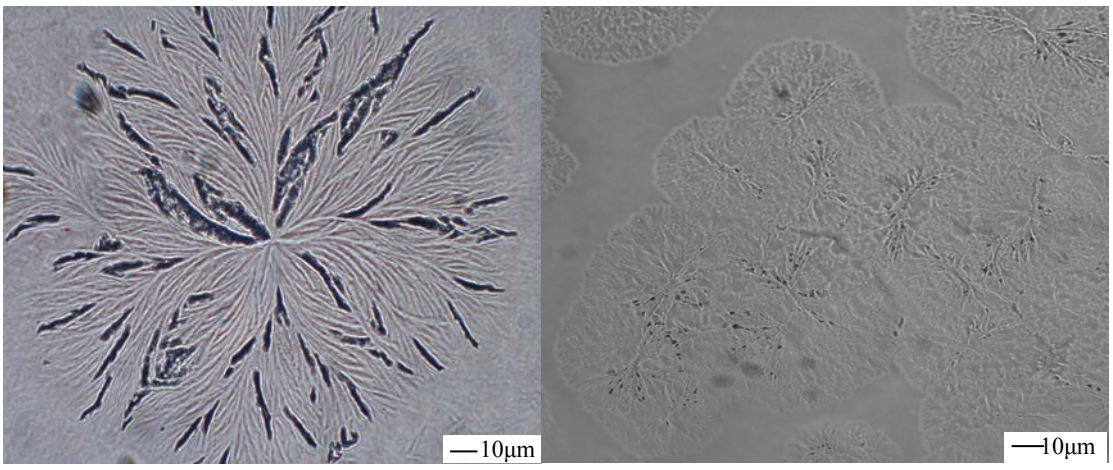

(a) (b)

Fig. 9. Optical micrographs showing spherulites developed in (a) pure PP in which lamellae radiate outward from the center and (b) PP-Ag mixture in which lamellae form a sheaf-like structure.

Numerous bundles of the developing lamella having rod-like structure can be observed in the silver containing spherulites (Fig. 9(b)). The branching of lamella evolves into sheaf-like β-spherulites. In contrast, silver free PP speherulites having lamellae radiate outward from the center (Fig. 9(a)). SEM micrographs also reveal that the spherulites are nucleated on Ag particles (Figs.10(a) and (b)). The nucleation mechanism of Ag nanoparticle induced β-PP is rather complicated, further work is needed in future to elucidate this issue.

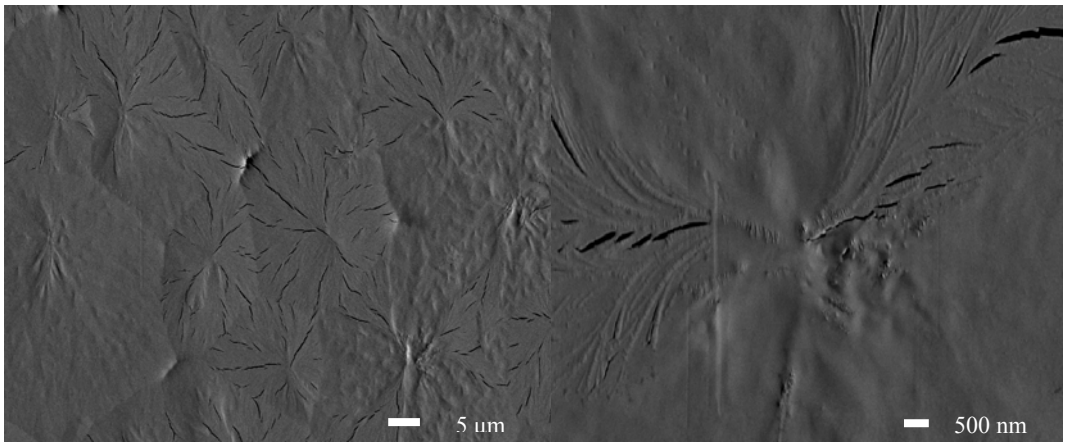

Fig. 10. (a) SEM micrograph of PP spherulites developed in PP-Ag mixture. (b) Higher magnification view of spherulites in PP-Ag mixture. Silver particles are indicated by arrows.

Mechanical Behavior

Figures 11 (a)-(c) show the effects of Ag nanoparticle addition on the tensile and impact properties of PP. As shown in Fig.11 (a), the impact strength increases rapidly with the Ag content up to 0.3 wt%. Thereafter, a considerable reduction in impact strength is observed with further increasing filler content, particularly at 1 wt%. The addition of 0.1 wt % Ag results in a sharp increase of impact strength to 4.8 kJ m^{-2} and this value is 20% higher than that of pure PP. The improvement of impact properties is associated with the formation of β-form PP due to the Ag additions [30, 31]. At 1.0 wt % Ag, the impact toughening effect diminishes due to the aggregation of Ag nanoparticles. Fig. 11 (b) reveals that there is little change of the tensile strength for PP/Ag composites with the Ag additions. The elongation at break of pure PP and its nanocomposites cannot be determined at a strain rate of 10 mm min^{-1} as these specimens do not fracture at such a low strain rate. Therefore, the specimens were strained at 50 mm min^{-1} in order to obtain the elongation at break values. The variation of elongation at break with Ag content is shown in Fig. 11 (c). The elongation at break of PP/0.1 wt% Ag is about twice of pure PP. This is attributed to the formation of the β-form induced by the Ag nanoparticles. Further increasing Ag content up to 1.0 wt% leads to a decrease in the elongation at break of PP. Fig.11 (a) and Fig.11 (c), the impact strength values of the composites with 0.1 and 0.3 wt% Ag are similar, but the elongation at break of former composite is higher. In general, the β-PP phase is beneficial in improving the tensile ductility and impact strength of polymer blends and composites. However, the β-PP phase content of PP/0.1 wt% and PP/0.3 wt % nanocomposites is nearly the same (Table 1), thus the differences

in impact and elongation behaviors of these composites are not directly related to β-PP. Impact and tensile measurements are tested under quite different strain rate conditions. The loading speed employed in impact test is much higher than that in tensile measurement. When the composites are tensile deformed, the uniformly dispersed silver nanoparticles carry the applied load at the early stage of tensile deformation. At the same time, the reinforcing Ag particles act as stress concentrators, thereby yielding a triaxial state of stress around them. Consequently, Ag nanoparticles would debond from the particle-PP interface, leading to the formation of small cavities or voids. With further deformation, fibrillation occurs in surrounding PP matrix, and the voids are elongated accordingly [32, 33].

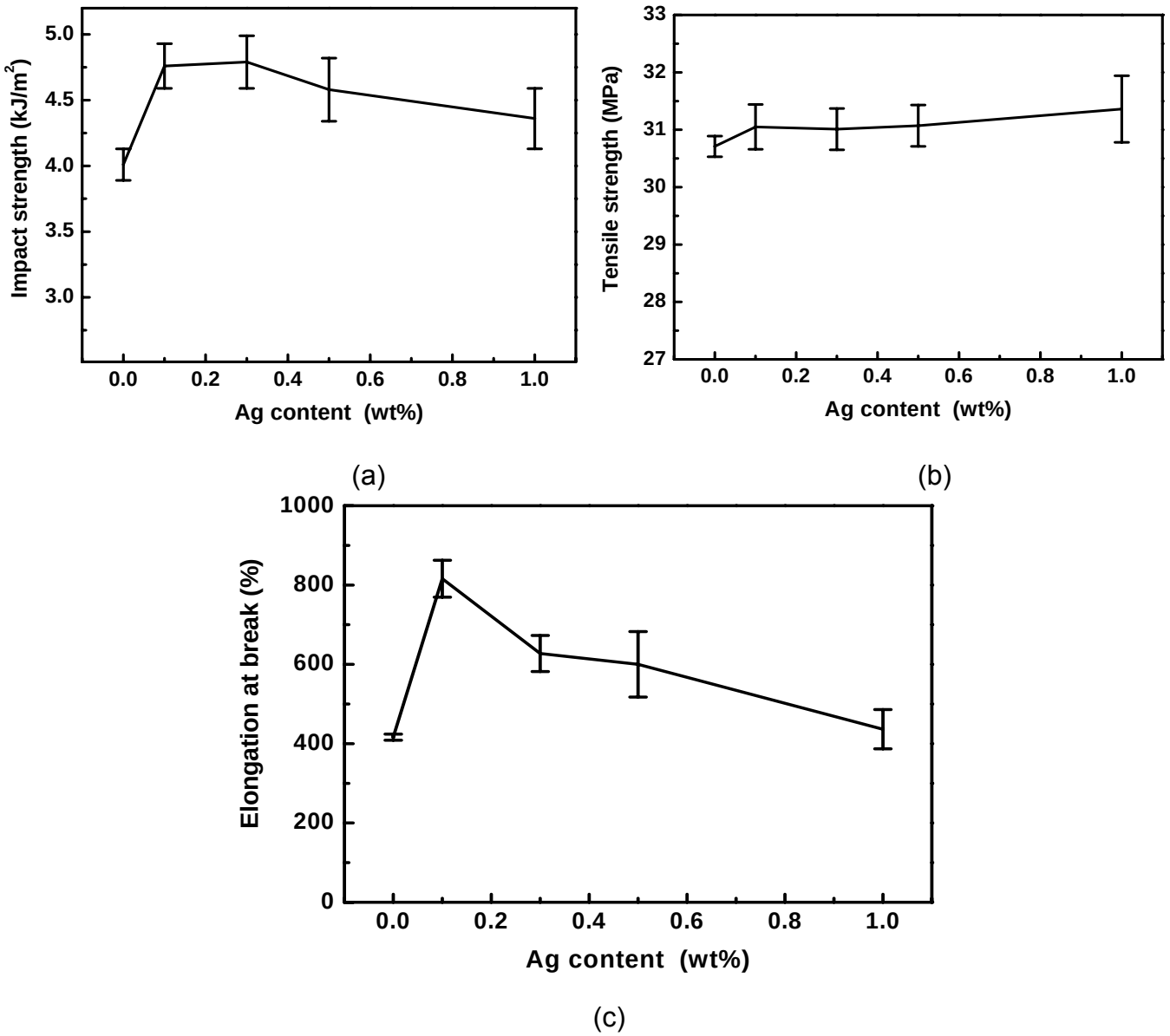

Fig. 11. Variations of (a) Izod impact strength, (b) tensile stress and (c) elongation at break with Ag content for PP nanocomposites.

A schematic diagram for tensile deformation is shown in Fig. 12. Thus the composite with higher silver content (i.e. 0.3 wt%) has higher stress concentrators and corresponding elongated voids. This leads to a lower value of elongation at break.

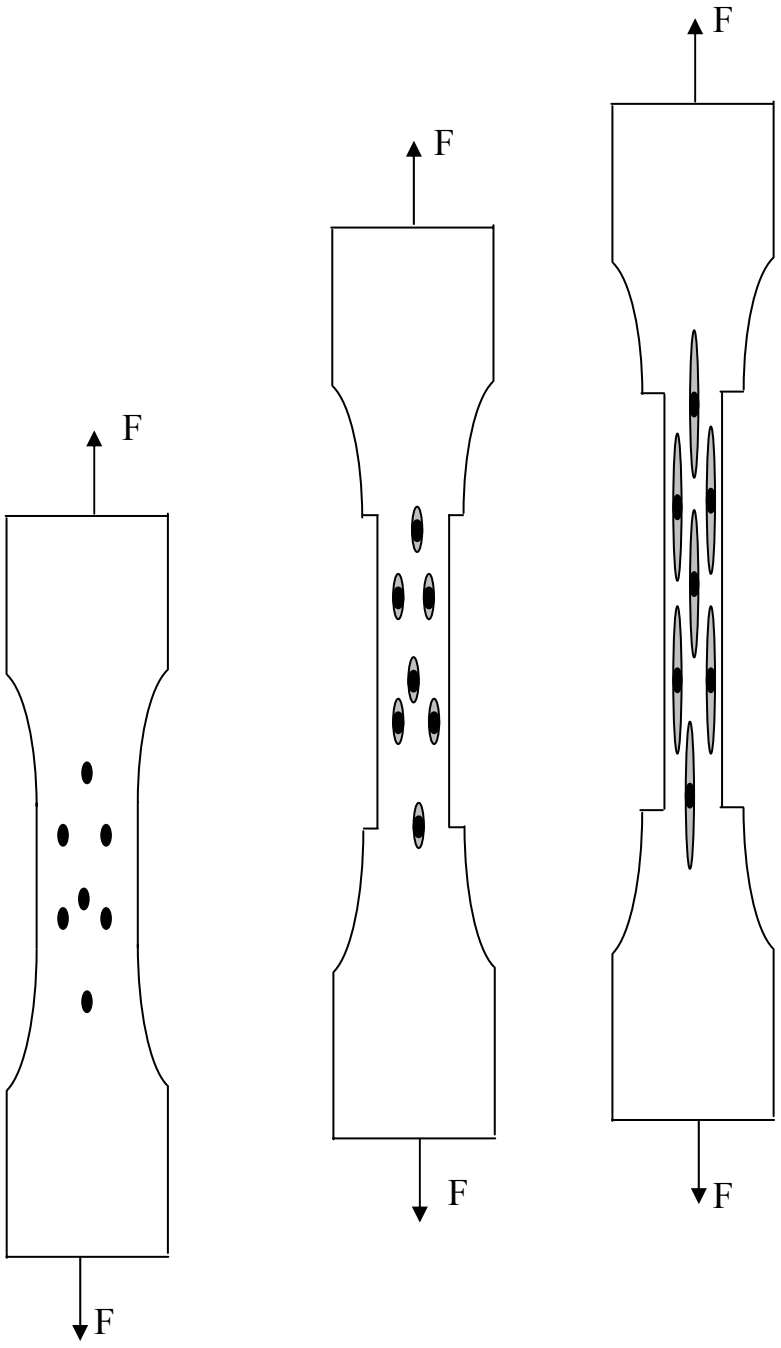

Fig. 12. A schematic diagram for tensile deformation.

It is well recognized that the nanoparticle additions are beneficial in enhancing the tensile strength and ductility as well as the impact strength of thermoplastics [34, 35]. However higher amounts of ceramic nanoparticles (2 -5 wt% SiO_2) are needed to achieve the tensile and impact toughening effects. It is interested to note that an improvement in the impact strength and tensile ductility of PP can be realized by adding a very small amount of Ag nanoparticles (0.1 wt%) in the present study. As

aforementioned, TEM observations revealed that Ag nanoparticles having large surface area are dispersed more uniformly within PP matrix. As a result, the applied load can be transferred more efficiently from the matrix to the reinforcement materials during tensile loading, thereby promoting a strengthening effect. The strengthening effect of Ag nanoparticles in the nanocomposites is offset by the formation of β- PP phase with lower yield strength. Therefore, the tensile strength of PP/Ag nanocomposites investigated shows little change with Ag content (Fig. 11 (b)).

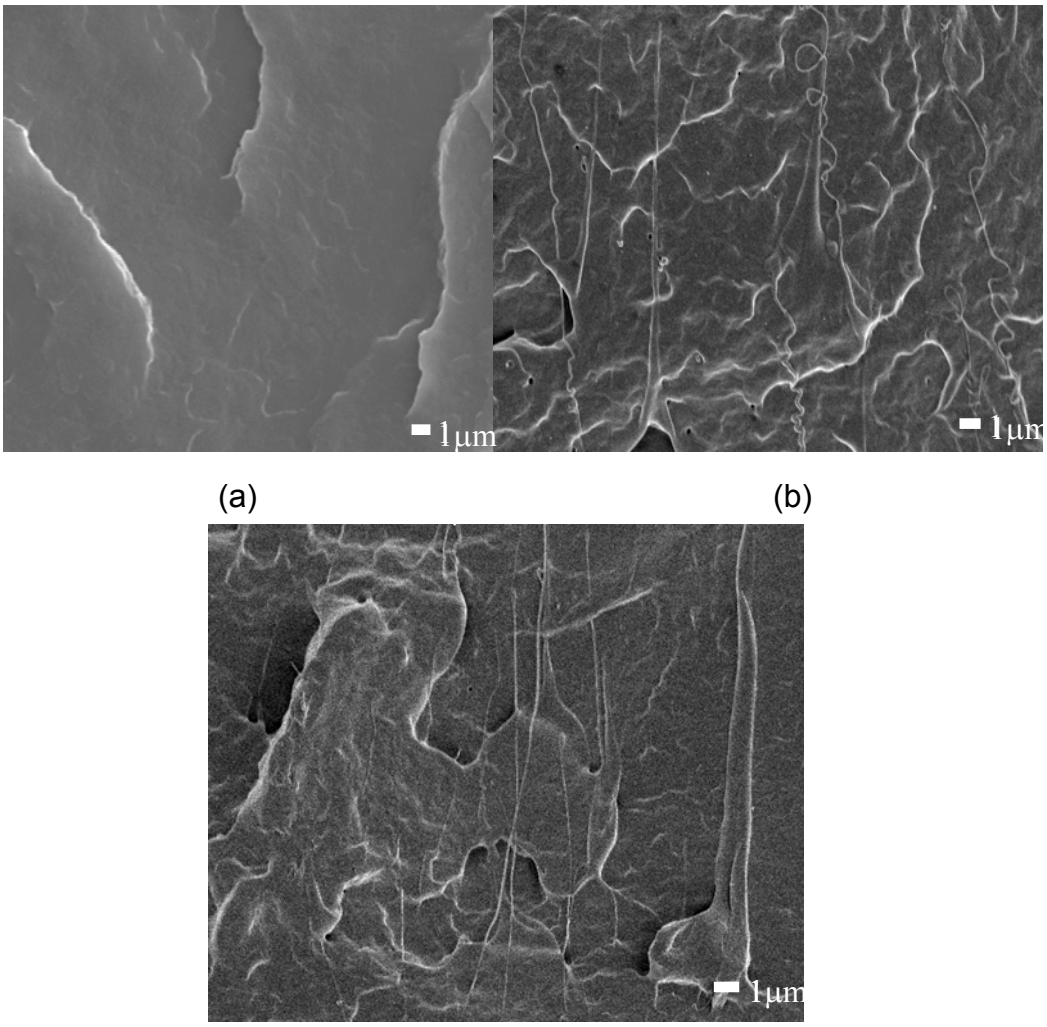

Fig. 13. SEM fractographs near the notch tip of (a) pure PP, (b) PP/0.1 wt% Ag and (c) PP/0.3 wt% Ag nanocomposites after impact tests

Figures 13 (a) – (c) are field-emission scanning electron fractographs taken near the notch tip of pure PP, PP/0.1 wt% Ag and PP/0.3 wt% Ag impact specimens. The fracture surface of pure PP is smooth and even, implying little energy is dissipated during the impact process (Fig. 13 (a)). From Figs.13 (b) and (c), numerous fibrillated zones can be observed in the fracture surface for PP/Ag nanocomposites. The fibrillation zone near the notch tip of the impact samples is caused by the β-PP. The β-form spherulites exhibit a distinct sheaf-like lamellar morphology in which the lamellar bundles are linked together by tie molecules of the amorphous phase. The lamellar bundles can be easily separated from each other by subjecting to mechanical loading, leading to the formation of microcrazes and microfibrils. Such

unique morphology of β-form spherulites renders the polypropylene to possess superior impact strength and tensile ductility [30, 31, 36].

Conclusions

PP nanocomposites filled with 0.1, 0.3, 0.5 and 1.0 wt% Ag nanoparticles were fabricated via melt-compounding process. The effects of Ag nanoparticle addition on the structure and mechanical properties of PP were studied. DSC results showed that the Ag nanoparticles act as a heterogeneous nucleation agents for β-PP on the basis of the presence of additional β-PP melting peak and higher temperatures of crystallization. The amount of β-PP phase formed in the PP/Ag nanocomposites was determined by the DSC and WXRD methods. WXRD measurement revealed that the relative amount of β-PP phase formed in the PP/Ag nanocomposites containing various filler contents is ~19 %. Such induced β-PP phase was beneficial in improving the impact strength and tensile ductility of the PP/Ag nanocomposites.

Experimental

Materials

Silver nanoparticles were purchased from Nanostructured & Amorphous Materials Inc. The Ag nanoparticles were dispersed ultrasonically for 10 min in an ethanol solution, then retrieved on a copper grid and examined in a transmission electron microscope (TEM; Philips CM20). Fig. 14 shows a typical TEM micrograph of Ag nanoparticles.

The TEM micrographs were analyzed using an image analysis software (SemAfore) for determination of the size distribution of Ag nanoparticles (Fig. 2). Isotactic polypropylene with a molecular weight M_w = 250,000 and a melt flow index of 12 g/10 min was obtained commercially from HMC Polymers Co., Ltd.

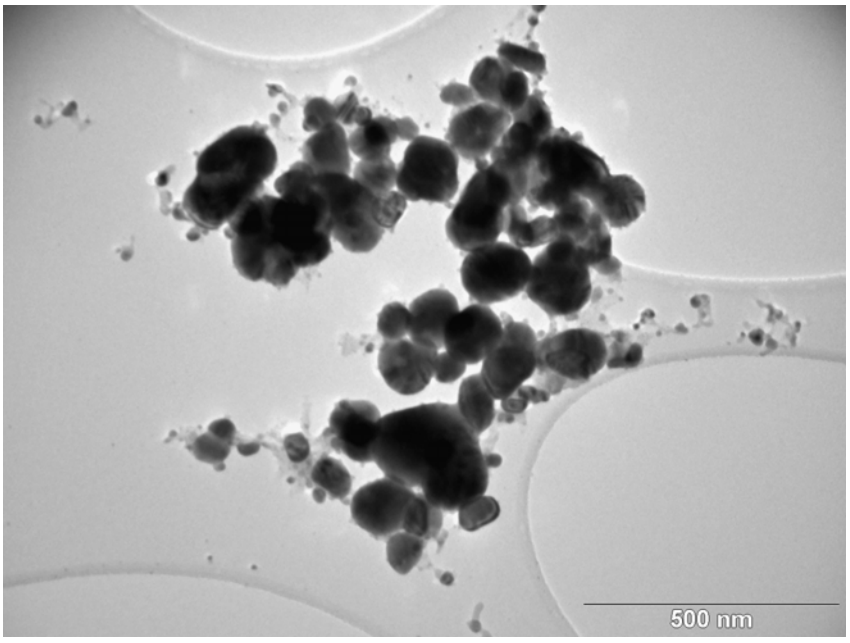

Fig. 14. TEM image of Ag nanoparticles.

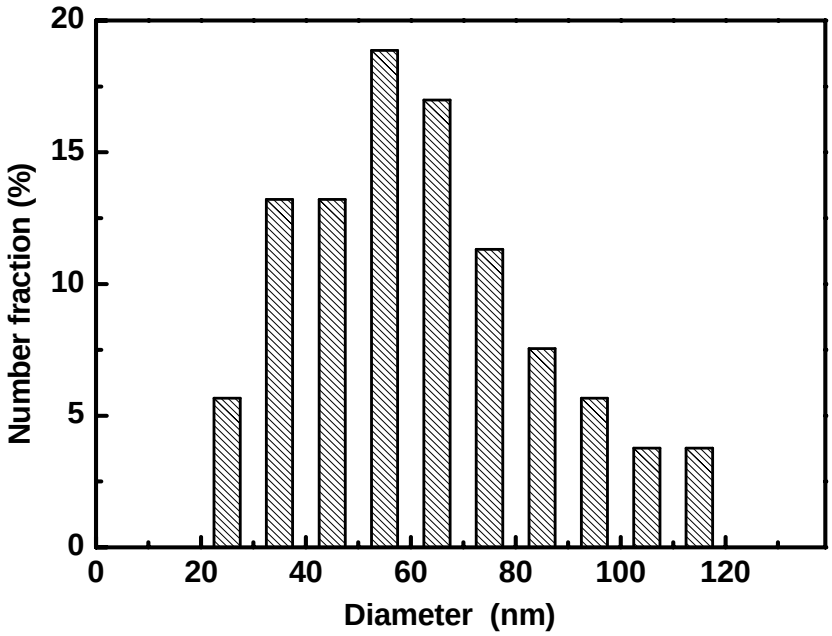

Fig. 15. Size distribution of Ag nanoparticles.

Sample Preparation

The PP nanocomposites containing 0.1, 0.3, 0.5 and 1wt % Ag were prepared via melt mixing in a twin-screw Brabender Plasticorder at 60 rpm. Due to a large density difference between PP and Ag nanoparticles, the nanoparticles tended to agglomerate near the bottom of container. To achieve uniform dispersion of the Ag nanoparticles in PP matrix, Ag powders and dried PP pellets were initially tumbled in small isolated bottles (125 ml). This process facilitated Ag nanoparticles to coat the PP pellets more evenly. Then the mixed components were fed into the hopper of an extruder. The melt blending temperature profile of the extruder was set at 220-230-220-190 °C. The extrudates were granulized upon exiting the pelletizer. Such pellets were fed into Brabender again to achieve more homogeneous blending. The products were also granulized and dried in an oven for 48 h at 80 °C before injection molding to the plaques of 3.2 mm thickness. The injection mold temperature was maintained at 40 °C, whereas the barrel zone temperatures were set at 235, 235 and 235 °C. Pure PP plaques were also processed under identical conditions for the purpose of comparison. The injection molded plaques were cut into the standard dog-bone tensile bars (ASTM D638) and Izod impact specimens.

Mechanical Measurements

Tensile tests were performed using an Instron tester (model 4206) at room temperature at a crosshead speed of 10 mm min^{-1}. The elongation at break for the specimens was obtained at a crosshead speed of 50 mm min^{-1}. Seven specimens of each composition were tested and the average values are reported. Izod Impact tests were carried out using a Ceast impact tester equipped with both personal computer and software at room temperature. Six specimens of each composition were used and the average values reported. The fracture surfaces of impacts specimens were

coated with a thin gold layer before being examined in a Jeol JSM 6335 field-emission scanning electron microscope (FESM).

Differential Scanning Calorimetry (DSC)

The melting and crystallization behavior of the samples were determined using a TA Instruments DSC (model 2910) under nitrogen atmosphere. The extruded pellets of ~ 5 mg were initially heated to 220 °C at a rate of 100 °C min^{-1}. They were held for 5 min at this temperature in order to eliminate previous thermal histories. Then the samples were cooled down to 20 °C at a rate of 10 °C min^{-1}, and finally heated again to 220 °C at the same rate.

X-ray Diffraction Measurement

Wide-angle X-ray diffraction (WXRD) measurements were performed with a Siemens D500 diffractometer equipped with Ni-filtered CuK_{α} radiation having a wavelength of 0.154 nm. The diffractometer was operated at 30 kV. The diffractograms were scanned in 2θ ranges at a rate of 0.02° s^{-1}. Both extrudates and injection-molded samples were used for the measurements.

Transmission Electron Microscopy

The dispersion of Ag nanoparticles in PP matrix was examined with a transmission electron microscope (TEM; Philips CM 20). Ultrathin specimens (~70 nm) were cut from the mid-section of injection-molded plaques using a microtome (Reichert Ultracut) under cryogenic conditions. The film were then retrieved onto copper grids.

Optical Microscopy

The morphology of PP and PP nanocomposites filled with Ag nanoparticles were observed with a polarizing optical microscope (Olympus BH2-UMA) equipped with a digital camera (Nikon DS-Fi1). The sample was sandwiched between two microscopic glass slides and placed on a hot stage. Then it was heated at 200 °C for 5 min to eliminate any previous thermal or mechanical history. The molten sample was then pressed into the thin film of about 0.1 mm and slowly cooled in air to room temperature.

To observe the morphology of spherulites developed in the composites during the early stage of crystallization, the following procedures were adopted. The silver particles were first dispersed ultrasonically in an ethanol solution for 10 min. The homogeneous suspension was dropped onto a microscopic glass slide. Then PP thin film of ~ 0.1mm thickness was placed on the slide and the PP-Ag mixture was heated to 180 °C to reach a molten state condition. The mixture was fast cooled to room temperature to prevent the growth of spherulites. For the purpose of comparison, pure PP thin film was also heated at 180 °C and rapidly cooled down to room temperature. Optical micrographs of slide samples were taken using a transmission optical microscope fitted with digital camera (Nikon DS-Fi1). The slide samples were further coated with gold prior to SEM observation.

References

[1] Collar, E. P.; Areso, S.; Laguna, O.; Garcia-Martinez, J. M. *J. Polym. Mater.* **1998**, 15, 237.
[2] Iroh, J. O.; Berry, J. P. *Polymer* **1993**, 34, 4747.

[3] Tjong, S. C.; Li, R. K. Y. *J. Vinyl. Add. Techol.* **1997**, 3, 89.
[4] Tselios, C.; Bikiaris, D.; Savidis, P.; Panayiotou, C.; Larena, A. *J. Mater. Sci.* **1999**, 34, 385.
[5] Joly, C.; Kofman, M.; Gauthier, R. *J. Macromol. Sci. Pure.* **1996**, A33, 1981.
[6] Collar, E. P.; Martinez, J. M. G.; Laguna, O.; Taranco, J. *J. Polym. Mater.* **1996**, 13, 111.
[7] Bikiaris, D. N.; Papageorgiou, G. Z.; Pavlidou, E.; Vouroutzis, N.; Palatzoglou, P.; Karayannidis, G. P. *J. Appl. Polym. Sci.* **2006**, 100, 2684.
[8] Chan, C. M.; Wu, J. S.; Li, J. X.; Cheung, Y. K. *Polymer* 2002, 43, 2981.
[9] Ma, C. G.; Rong, M. Z.; Zhang, M. Q. *Polym. Eng. Sci.* **2005**, 45, 529.
[10] Wu, C. L.; Zhang, M. Q.; Rong, M. Z. *Compos. Sci. Technol.* **2002**, 62, 1327.
[11] Norton, D. R.; Keller, A. *Polymer* **1985**, 26, 704.
[12] Lovinger, A. J.; Chua, J. O.; Gryte, C. C. *J. Polym. Sci. Pol. Phys.* **1977**, 15, 641.
[13] Dragaun, H.; Hubeny, H.; Muschik, H. *J. Polym. Sci. Pol. Phys.* **1977**, 15,1779.
[14] Binsberg, F. l. *Polymer* **1970**, 11, 253.
[15] Varga, J. J. Macromol. Sci. Phys. **2002**, B41, 1121.
[16] Yu, D. G.; Teng, M. Y.; Chou, W. L.; Yang, M. C. *J. Membrane. Sci.* **2003**, 225,115.
[17] Jeong, S. H.; Yeo, S. Y.; Yi, S. C. *J. Mater. Sci.* **2005**, 40, 5407.
[18] Mezghani, K.; Phillips, P. J. *Polymer* **1995**, 36, 2407.
[19] Varga, J. *J. Therm. Anal. Calorim.* **1989**, 35, 1891.
[20] Samuels, R. J. *J. Polym. Sci. Pol. Phys.* **1975**, 13, 1417.
[21] Edward, P. M. *Polypropylene*, Munich: Hanser Publishers 1996.
[22] Brandrup, J.; Immergut, E. H. *Polymer Handbook*, New York: John Wiley & Sons Inc. **1989**.
[23] Chae, D. W.; Kim, B.; C. *Macromol. Mater. Eng.* **2005**, 290, 1149.
[24] Turner-Johes, A.; Aizlewood, J. M.; Beckett, D. R. *Makromol. Chem.* **1964**, 75, 134.
[25] Mo, Z. S.; Zhang, H. F. *Structure of crystalline polymers by X-Ray diffraction*, Beijing: Science Publisher **2003**.
[26] Stocker, W.; Schumacher, M.; Graff, S.; Thierry, A.; Wittmann, J. C.; Lotz, B. *Macromolecules* **1998**, 31, 807
[27] Mathieu, C.; Thierry, A.; Wittmann, J. C.; Lotz, B. *J.Poly. Sci. Part B: Polym. Phys.* **2002**, 40, 2504
[28] Wittmann, J. C.; Lotz, B. *Prog. Polym. Sci.* **1990**, 15, 909
[29] Garbarczyk, J.; Paukszta, D. *Polymer* **1981**, 22, 562.
[30] Tjong, S. C.; Shen, J. S.; Li, R. K. Y. *Polym. Eng. Sci.* **1996,** 36, 100.
[31] Tjong, S. C.; Shen, J. S., Li, R. K. Y. *Polymer* **1996**, 37, 2309.
[32] Zuiderduin, W.C.J.; Westzaan, C.; Hue´tink, J.; Gaymans, R.J. *Polymer* **2003**, 44, 262.
[33] Bartczak1a, Z.; Argona, A.S.; Cohena, R.E.; Weinbergb, M. *Polymer* **1999**, 40, 2347.
[34] Bikirias, D. N.; Vassilou, A.; Pavlidou, E.; Karayannidis, G. P.; *Eur. Polym. J.* **2005**, 41, 1965.
[35] Qu, Y.; Yang, F.; Yu, Z. Z.; *J. Polym. Sci. Pol. Phys.* **1998**, 36, 789.
[36] Chu, F.; Yamaoka, T.; Ide, H.; Kimura, Y.; *Polymer* **1994**, 35, 3442.